

# Learning Single-View 3D Reconstruction with Adversarial Training

Pedro O. Pinheiro  
Element AI

Negar Rostamzadeh  
Element AI

Sungjin Ahn  
Rutgers University

## Abstract

*Single-view 3D shape reconstruction is an important but challenging problem, mainly for two reasons. First, as shape annotation is very expensive to acquire, current methods rely on synthetic data, in which ground-truth 3D annotation is easy to obtain. However, this results in domain adaptation problem when applied to natural images. The second challenge is that it exists multiple shapes that can explain a given 2D image. In this paper, we propose a framework to improve over these challenges using adversarial training. On one hand, we impose domain-confusion between natural and synthetic image representations to reduce the distribution gap. On the other hand, we impose the reconstruction to be ‘realistic’ by forcing it to lie on a (learned) manifold of realistic object shapes. Moreover, our experiments show that these constraints improve performance by a large margin over a baseline reconstruction model. We achieve results competitive with the state of the art using only RGB images and with a much simpler architecture.*

## 1. Introduction

Humans can easily understand the underlying 3D structure of scenes and objects from single images. This is a hallmark of a human visual system and it is an essential step towards higher level visual understanding. This is an extremely ill-posed problem because a single image does not contain enough information to allow 3D reconstruction. Therefore, a machine vision system needs to rely on priors over the shape to infer 3D structure.

Efficient and effective 3D prototyping plays an important role in many different fields, such as virtual/augmented reality, architecture, robotics and 3D printing to name a few. Perhaps more importantly, studying 3D object representations could bring insights on how this information is encoded in intermediate and higher-level visual cortices [51, 26].

Traditional reconstruction methods rely on multiple images of same object instance [28, 4, 6, 37, 14]. These methods possess two strong limitations due to some key assumptions [8]: (i) it requires a large number of views to achieve reconstruction, (ii) the objects’ appearance are expected to be Lambertian (*i.e.* non-reflective) and their albedos are supposed to be non-uniform (*i.e.*, rich of non-homogeneous textures).

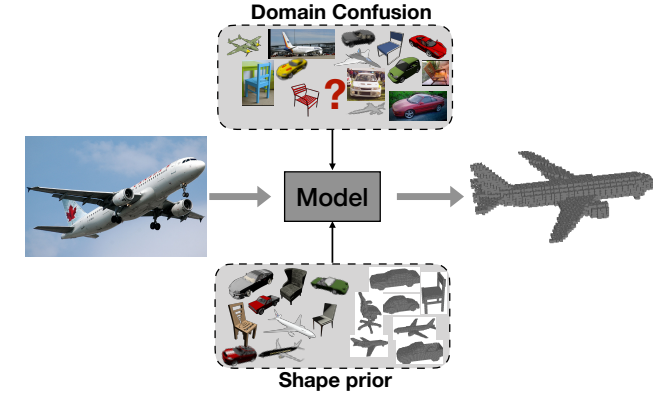


Figure 1: We propose a framework for (natural) single-view 3D reconstruction exploiting adversarial training in two ways. These constraints are achieved with additional loss terms. We impose domain confusion between natural and rendered images (top) and exploit shape priors to force reconstructions to look realistic (bottom).

Another way to achieve 3D reconstruction is to leverage knowledge from object’s appearance and shape. The main advantages of relying on *shape priors* is that we do not need to rely on accurate feature correspondences across different views. In this case 3D reconstruction can, in principle, be done from a single-view 2D image (assuming the priors are rich enough).

Recently, there has been a growing interest in learning-based approaches to tackle the problem of predicting the canonical shape of an object from a single image [24, 8, 16, 39, 52, 22, 46, 32, 42, 45, 47, 53]. Two technical advances were responsible for this surge: (i) the easy access to large-scale 3D Computer-Aided Design (CAD) repositories, such as ShapeNet [7], Pascal3D+ [50], ObjectNet3D [49], Pix3D [38] and (ii) advances in deep learning techniques [17].

Most of these methods contain a similar high-level architecture that regresses a 3D shape from (rendered) images: an encoder that transforms a 2D image into a latent representation and a decoder that reconstruct the 3D representation. They differentiate in how constraints from 3D world are imposed, *e.g.*, [8, 52, 42] force multi-view consistency to learn the 3D representation, while [45, 47] make use of 2.5D sketches. These approaches use a large number of CAD models to leverage shape priors (either making explicit use of 3D representation or not).

Single-view 3D reconstruction is a very ill-posed problem. In order to learn strong shape priors to be able to infer 3D structure, deep learning methods require a large amount of 3D object annotations. However, acquiring good 3D object annotation from natural images is an extremely challenging endeavor. Most deep learning approaches, therefore, make use of synthetic images (which can be rendered easily if a proper 3D representation is given).

Convolutional neural networks (CNN) [29] are known to perform sub-optimally when the data distribution of inputs changes, a problem known in the computer vision literature as *domain shift* [41]. For this reason, applying a CNN-based 3D reconstruction method on natural images tends to worsen its performance if compared to synthetic images (generated with the same rendering configurations).

In this paper, we introduce a method to improve the performance of reconstruction models in natural images, where proper 3D labels are very difficult to acquire. To achieve this goal, we impose two constraints on the network’s reconstruction loss (expressed as additional loss terms) based on shape prior learned from large 3D CAD repository (see Figure 1).

First, inspired by the domain adaptation literature [9, 15], we force the encoded 2D features to be invariant with respect to the domain they come from (rendered or natural). This way, a decoder trained on synthetic images will naturally perform better on real images. Second, we constraint the encoded 2D features to lie in the manifold of realistic objects shapes. This constraint forces the decoded 3D reconstruction to look more realistic. These two loss terms are characterized through adversarial training [18, 15], an active research topic.

Our main contributions can be summarized as follows: (i) we propose a model and a loss function that exploit learned shape priors to improve performance of natural image 3D reconstructions (using adversarial training in two different ways), and (ii) we show that this method boost results over a simple reconstruction model baseline and achieve results competitive with state of the art on different datasets. Importantly, contrary to competitive methods, our approach uses only RGB images as input and has a much simpler architecture.

The rest of the paper is organized as follows: Section 2

presents related work, Section 3 describes how we learn the shape prior and leverage it in two different ways for learning reconstruction, and Section 4 describes our experiments in different datasets. We conclude in Section 5.

## 2. Related Work

**Single-view 3D reconstruction.** Traditional reconstruction methods rely on multiple images of same object instance to achieve reconstruction [28, 4, 6, 37, 14]. Recently, data-driven approaches to 3D reconstruction from single image have appeared. These methods can roughly be divided into two types: (i) those that explicitly use 3D structures [16, 8, 46, 13, 45, 48] and (ii) those that use other sources of information to infer the 3D structure [44, 24, 52, 22, 20, 6, 42, 53].

These approaches, based on deep learning techniques, usually share a similar (high-level) architecture: an encoder that maps 2D (rendered) images into a latent representation and a decoder that maps this representation into a 3D object. They tend to differ in the way 3D world constraint are imposed. For instance, [8, 52, 52, 42, 20, 22, 27] force multiview consistency to learn the 3D representation, while [44, 24, 23] leverage keypoints and silhouette annotations. Other approaches [45, 47] leverage 2.5 sketches (surface normals, depth and silhouette) information to improve prediction.

Contrary to all these methods, our approach does not use any additional information besides RGB images. However, in addition to rendered images, we also use unlabeled natural images (which are easy to acquire). We note that our contributions are independent of the encoder and decoder architecture (as long as they are differentiable), and could be applied in many of these more powerful encoder-decoder architectures.

**Domain Adaptation.** The difficulty to acquire 3D annotations for natural images forces reconstruction models to learn form rendered images. It is well known in the literature [41, 9] that the performance of a model drops if applied in data coming from a distribution different from the one used during training. Ganin *et al.* [15] deal with this issue by forcing domain confusion (between two domains) through an adversarial objective. Many works have been dealing with domain adaptation from synthetic to real for image classification [34, 35, 33, 36]. In this work, we borrow ideas from domain adaptation literature to impose domain confusion in a similar way as these previous work. We consider, however, the more challenging problem of 3D reconstruction instead of classification.

**Shape Priors.** Reconstruction of 3D structure from single-view images requires strong priors about object’s

shape. Many works focus on better capturing the manifold of realistic shapes. Non-deep approaches had focus on low-dimensional parametric models [3, 24]. [16, 30] use CNNs to learn a common embedding space for 2D rendered images and 3D shapes. Other methods rely on generative modeling to learn shape prior, *e.g.*, [48] use deep belief nets to model 3D representations, [22, 6, 11] consider variants of variational autoencoders and [46] use a variant of GANs [18] to capture the manifold of shapes.

A few works use adversarial training for single-view 3D reconstruction. Gwak *et al.* [20] use GANs to model 2D projections instead of 3D shapes. More similar to our work, Wu, Zhang *et al.* [47] use adversarial training techniques to impose reconstructions to look more natural. They use the discriminator of a pre-trained 3D GAN [46] to determine whether a shape is realistic. This approach is similar in principle to one of our contributions. It is, however, implemented in very different way. The input to the discriminator is a high dimensional 3D shape, which makes the training to be very unstable. In our method, the input is a single vector in a low-dimensional space.

### 3. Method

In our reconstruction setting, we are interested in predicting a *voxel occupancy grid*  $v^n \in \mathcal{V} \subset \{0, 1\}^{d_v \times d_v \times d_v}$  from a canonical view of a natural image  $x^n \in \mathcal{I}^n \subset \mathbb{R}^{3 \times H \times W}$ . At training time, we have access to a large repository of 3D CAD objects, where pairs of rendered images and occupancy grid  $\mathcal{D}_{rend} = \{(x_i^r, v_i)\}_{i=1}^{N_r}$  are drawn from a distribution  $p_r(x, v)$ , and unlabeled natural images,  $\mathcal{D}_{nat} = \{x_j^n\}_{j=1}^{N_n}$ , from a different distribution  $p_n(x, v)$ . We note that during training the model has access to natural images (which are easy to acquire), but not their voxel occupancy grid (which are very difficult to gather).

The proposed method, dubbed *Reconstruction Adversarial Network* (RAN), is composed of two components: (i) a *shape autoencoder*, responsible for learning a rich latent representation of 3D objects and (ii) a *reconstruction network*, responsible for inferring the voxel occupancy grid from a 2D image.

The shape autoencoder is made of an encoder  $E$  and a decoder  $D$  containing 3D convolutions and downsampling and upsampling layers, respectively. The encoder maps 3D voxel representation  $v \in \mathcal{V}$  into a low-dimensional embedding representation  $e \in \mathcal{E} \subset \mathbb{R}^{d_e}$ . The decoder maps a data point in the latent space back to a 3D voxel representation. We train the autoencoder by minimizing the  $L_2$  reconstruction loss.

Since the shape autoencoder is trained with true 3D voxel representations, the learned latent representation lies in the *shape manifold*  $\mathcal{E}$ , containing low-dimensional embeddings of ‘realistic’ shapes. This component is trained prior to the training of the reconstruction network. The shape prior in-

formation is implicitly encoded in this rich representation space.

The reconstruction network also possesses an encoder-decoder architecture. The encoder  $f$ , parameterized by  $\theta_f$ , is responsible to transform a 2D image into an embedding space from which a voxel representation can be reconstructed with a decoder. At inference time, the reconstruction network is the sole network used to predict the voxel occupancy of a given natural test image.

The model is trained in a way that the encoder mapping  $f : \mathcal{I} \rightarrow \mathcal{E}$  can, at the same time: (i) reconstruct a voxel representation given a rendered image, (ii) be indistinguishable w.r.t. the domain that the image comes from (either synthetic or real) and (iii) stay in the manifold of ‘realistic’ shapes (learned with the shape autoencoder). To impose these constraints, we define and add the relevant terms to the loss function. Figure 2 shows an overview of the approach.

The reconstruction loss is applied to tuples of rendered images and occupancy grids (from  $\mathcal{D}_{rend}$ ) and is defined as:

$$\mathcal{L}_{rec}(\theta_f) = \mathbb{E}_{(x^r, v) \sim p_r} \|D^*(f(x^r)) - v\|_2^2, \quad (1)$$

where  $D^*$  is the shape decoder. The star indicates that we opt to *not* update the decoder parameters at this training stage. This design choice, combined with the constraint imposed by the third loss, forces the image representations to lie on the manifold of ‘realistic’ shapes.

In the rest of this section, we show how we leverage adversarial training techniques and (learned) shape prior to improve performance of natural image 3D reconstruction.

#### 3.1. Confusing Image Domains

It is well known that machine learning algorithms suffer from domain shift [41]. Therefore, a model trained to reconstruct voxels from rendered images performs sub-optimally when applied to natural ones. As we are interested in natural image reconstruction, we borrow ideas from unsupervised domain adaptation literature [15] to alleviate this issue.

Theoretical studies [2, 1] suggest that a good cross-domain representation one in which input domain cannot be easily identified. We implement such domain confusion by mapping cross-domain features into a common space through adversarial training. We cast this problem as a minimax game between a domain classifier and feature encoders. That is, we encourage the feature encoder to learn features  $f(x)$  that maximize the domain confusion between natural and rendered images.

We consider a discriminator  $D_{img}$ , parameterized by  $\theta_{img}$ . The discriminator that classifies the domain of a given feature vector, is optimized by the standard adversarial clas-

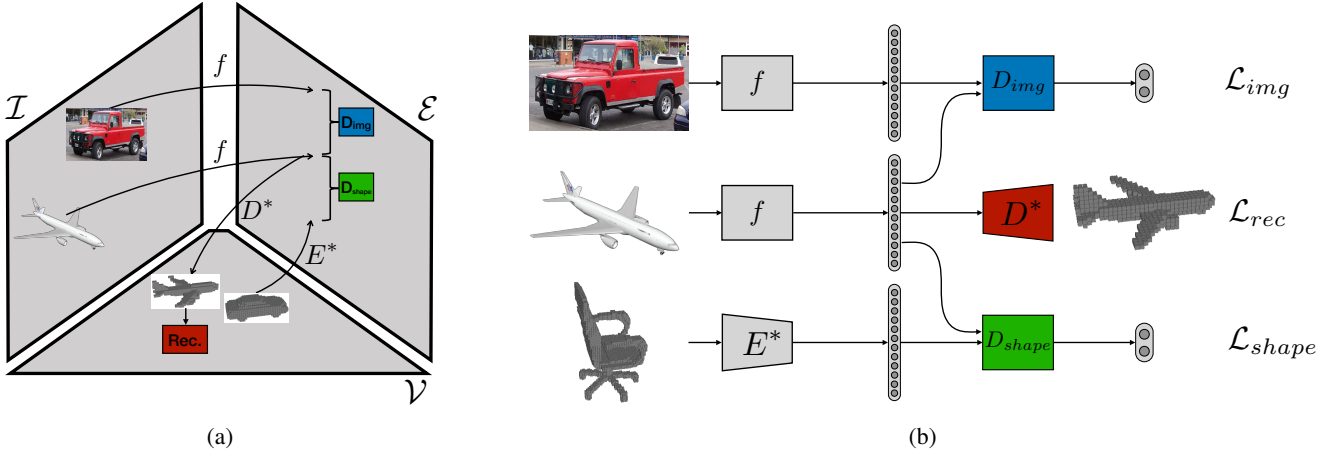


Figure 2: (a) The reconstruction network maps an image to a rich embedding space  $\mathcal{E}$  which is then decoded into a 3D shape with the shape decoder  $D^*$ . The two constraints are imposed on the embedding space with the help of two discriminators:  $D_{img}$  imposes image domain confusion and  $D_{shape}$  forces the embeddings to lie on the shape manifold. (b) Overview of the proposed architecture.

sification loss as follows:

$$\begin{aligned} \mathcal{L}_{img}(\theta_f, \theta_{img}) = & -\mathbb{E}_{x^r \sim p_r} \log D_{img}(f(x^r)) + \\ & -\mathbb{E}_{x^n \sim p_n} \log (1 - D_{img}(f(x^n))) . \end{aligned} \quad (2)$$

We achieve domain confusion by applying Reverse Gradient algorithm [15], which optimizes the parameters  $\theta_f$  to maximize the discriminator loss directly, while  $\theta_{img}$  minimizes it.

### 3.2. Exploiting Shape Priors

A lot of inherent ambiguity exists in single image reconstruction. Multiple objects exists that can explain a single view. For this reason, as noted by Wu, Zhang *et al.* [47], 3D reconstruction with only supervised loss tends to predict unrealistic mean shapes.

We characterized a representation to be ‘realistic’ if it belongs close to the manifold created by the (learned) shape autoencoder. We argue that if the feature of a single 2D image  $f(x)$  lies in the same manifold, a realistic reconstruction can be achieved by leveraging the decoder of the shape autoencoder.

The third component of our loss,  $\mathcal{L}_{shape}$ , imposes this constraint by penalizing the model if the distribution of 2D embeddings does not match that of the points in the shape manifold. We rely on the learned shape autoencoder to sample these points. Again, we use adversarial training to optimize the loss.

Similar to Equation 2, we train a discriminator  $D_{shape}$  (parameterized by  $\theta_{shape}$ ) to classify whether a sample is drawn from a 2D encoding representation or from the shape manifold. Samples from the shape manifold are generated

by sampling voxel instances from ShapeNet and mapping them to the  $\mathcal{E}$ , using the learned shape encoder  $E^*$ . As before, the star means that the parameters of the encoder are kept unchanged during this stage of training. This way, we guarantee the encoded samples lie on the learned manifold.

Learning is achieved my minimizing the following loss:

$$\begin{aligned} \mathcal{L}_{shape}(\theta_f, \theta_{shape}) = & -\mathbb{E}_{x^r \sim p_r} \log D_{shape}(f(x^r)) + \\ & -\mathbb{E}_{v \sim p_r} \log (1 - D_{shape}(E^*(v))) . \end{aligned} \quad (3)$$

As before, the parameters  $\theta_{shape}$  are optimized to minimize this loss while the parameters  $\theta_f$  maximized it, therefore, forcing the 2D embeddings to lie on the shape manifold.

### 3.3. Training Details

The training procedure is done in two stages.

We start by training the shape autoencoder to learn shape priors. As we want to capture the intrinsic shape complexity of different objects, we train the model using the full ShapeNet dataset. The shape encoder  $E$  is composed of four 3D convolutional layers, each followed by a max-pooling and ReLU [31] non-linearity. The first layer contains  $5 \times 5$  filters while the remaining have  $3 \times 3$ . The number of hidden units are 32, 64, 128 and 256 respectively. Similarly, the shape decoder  $D$  has four convolution layers, but instead of max-pooling, we use bilinear upsampling. The dimension of the latent representation is 256. We train the model with Adam [25] optimizer and a learning rate of  $10^{-3}$ . Once training converges, we freeze the

parameters of the encoder and the decoder and use them in the reconstruction step.

The architecture of the reconstruction network is shown on Figure 2b. The parameters of network  $f$  are initialized with a ResNet-50 [21] that was pre-trained to perform classification on ImageNet dataset [10]. We replace the classification layer by a randomly initialized layer that outputs a 256-dimensional vector.

The two discriminators  $D_{img}$  and  $D_{shape}$  map the embedded features to the probability of which domain the input comes from (modeled by a softmax [5]). We use two fully-connected layers of dimension 1024, followed by ReLU. We choose not to share but have different set of parameters between the two discriminators because it performs slightly better in practice.

Finally the model is optimized to learn 3D representations that are domain-invariant and that lie in the manifold from the prior of realistic shapes. Consequently, our final goal is to optimize the following objective:

$$\begin{aligned} \min_{\theta_f} \max_{\theta_{img}, \theta_{shape}} & \mathcal{L}_{rec}(\theta_f) \\ & - \lambda_i \mathcal{L}_{img}(\theta_f, \theta_{img}) \\ & - \lambda_s \mathcal{L}_{shape}(\theta_f, \theta_{shape}), \end{aligned} \quad (4)$$

where  $\lambda_i$  and  $\lambda_s$  are balance parameters between the loss terms. We chose  $\lambda_i$  and  $\lambda_s$  to be 0.001 and 0.1, respectively. To optimize, we used Adam with learning rate  $10^{-4}$ .

## 4. Experiments

In this section, we start by comparing the performance of RAN with other methods on the problem of single-view reconstruction from natural images. We show results in two important datasets: the recently released Pix3D [38] and PASCAL 3D+ [50]. Then, we study how RAN behaves with respect to the different loss terms. Finally, we analyze the learned representation and show qualitative results that corroborates with the notion of domain confusion and shape manifold.

### 4.1. Experimental Setup

**Shape prior.** In the first stage of training, we learn shape prior by training the shape autoencoder. The autoencoder is trained to reconstruct voxel representation of objects from ShapeNet dataset [7] (we use the ShapeNetCore subset). This dataset contains over 50k object instances of 55 categories. We use the voxel representation with resolution  $32^3$  (a downsampled version of the voxels provided by the official repository). We consider the same trained shape autoencoder in all the presented experiments.

**Render Data.** The second training stage is responsible for inferring shape representation from a single-view image.

In this step, we make use of both natural and rendered 2D images.

For each object in ShapeNet, we render 30 images with random and unconstrained viewpoints.

We use Blender<sup>1</sup> for all our renderings. Since we evaluate the model in natural images, we use all rendered data for training.

**Evaluation metrics.** We evaluate the performance of our method using two metrics: Intersection over Union (IoU) and Chamfer Distance (CD). The metric IoU measures the similarity between ground-truth and (discretized) reconstruction voxels. This is the 3D extension of the common metric (of same name) used in segmentation. The Chamfer distance between two point clouds  $P_1, P_2 \subset \mathbb{R}^3$  is defined as:

$$CD(P_1, P_2) = \frac{1}{|P_1|} \sum_{x \in P_1} \min_{y \in P_2} \|x - y\|_2 + \frac{1}{|P_2|} \sum_{x \in P_2} \min_{y \in P_1} \|x - y\|_2. \quad (5)$$

For each point in each set, CD finds the closest point (in the other set) and average the distances. Since our algorithm works with voxel occupancy, we first sample points in the voxel isosurface before computing CD. It is shown by Sun and Wu *et al.* [38] that CD better correlates with human perception. For fair comparison, in the following sections we use the same evaluation code provided by the authors of Pix3D<sup>2</sup>.

### 4.2. Comparison to Other Methods

**Reconstruction on Pix 3D.** Pix3D is a large-scale benchmark of diverse image-shape pairs with pixel-level 2D-3D alignment. A significant part of the dataset is chairs because they are common and highly diverse. Following the previous works [38, 47], we evaluate our approach on the 2,894 untruncated and unoccluded ‘chair’ images.

During training, the reconstruction network has access to synthetic ShapeNet renderings (and their corresponding voxel ground-truth) and unlabeled natural images of ‘chair’ category (we use the natural images of the PASCAL 3D+ r1.1, which contains also ImageNet images). Figure 3 shows the qualitative results of reconstructions generated by our approach. As illustrated in this figure, RAN is able to reconstruct even in situations of strong self-occlusion.

Table 1 compares the performance of our approach with different methods on the Pix3D dataset. We show results on both IoU (higher is better) and CD (lower is better) metrics. Results from other models are taken from Wu, Zhang *et al.* [47]. It is important to mention that these methods use different types of data during training. For instance, PSGN [13] and AtlasNet [19] require ground-truth

<sup>1</sup><http://www.blender.org/>

<sup>2</sup><http://pix3d.csail.mit.edu/>

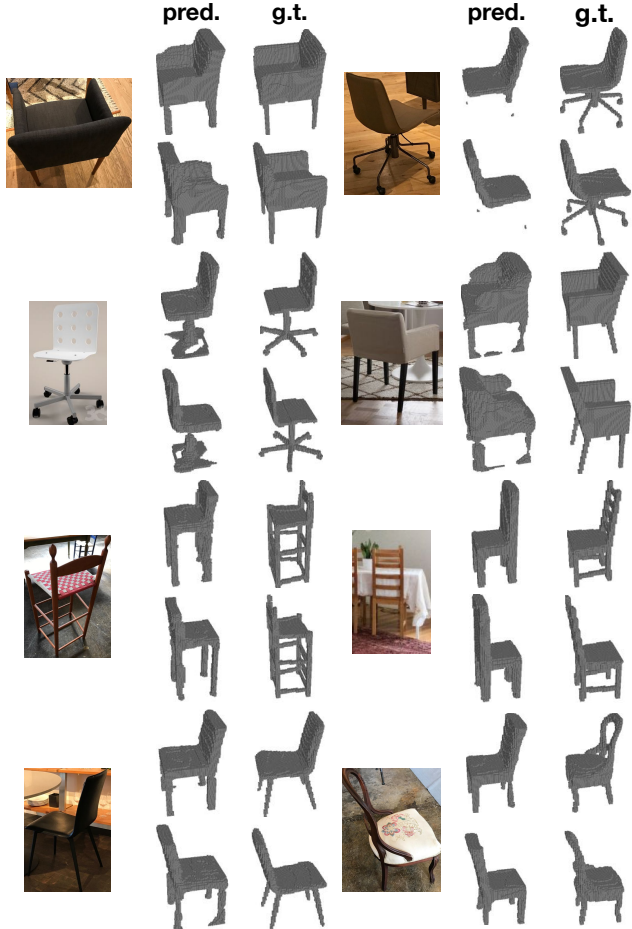


Figure 3: 3D reconstruction from single image on Pix3D dataset [38]. For each image, we show the predicted and the ground-truth voxel representations. Our method is capable of learning shape with very different appearances. We show two different views for each 3D representation.

masks as input. MarrNet [45], DRC [42] and ShapeHD [47] use depth, surface normals and silhouettes during training. RAN achieves competitive results using only RGB images as input and with a much simpler architecture.

**Reconstruction on Pascal 3D+.** PASCAL 3D+ [50] provides annotations for (rough) 3D shape of different rigid object instances from PASCAL VOC 2012 [12]. Each category has a small set of about 10 CADs per category.

Similar to most of the recent works, we do not use any of the PASCAL 3D+ training set. We use the CAD annotations only for benchmarking purposes. As discussed in Tulsiani *et al.* [42], using the small set of CADs for both training and test would bias the model toward those samples and therefore is not a recommended benchmark protocol.

	IoU	CD
3D-R2N2[8]	0.136	0.239
3D-VAE-GAN [46]	0.171	0.182
PSGN <sup>†</sup> [13]	-	0.199
MarrNet <sup>†</sup> [45]	0.231	0.144
DRC <sup>†</sup> [42]	0.265	0.160
AtlasNet <sup>†</sup> [19]	-	0.126
ShapeHD <sup>†</sup> [47]	0.284	0.123
RAN	0.237	0.136

Table 1: Single-view 3D reconstruction results on Pix3D. We show results on both IoU and CD metrics.<sup>†</sup> Methods using additional information during training. PSGN and AtlasNet require ground-truth mask as input. MarrNet, DRC and ShapeHD use 2.5 sketches to guide training. Our approach only considers (easily available) natural images during training. We show competitive results in both metrics.

We train our model in the categories that are present in both Pascal3D+ and ShapeNet: ‘aeroplane’, ‘bus’, ‘car’, ‘chair’, ‘motorbike’, ‘train’ and ‘tv monitor’. During training, our approach uses ShapeNet rendered images-voxels tuples and natural images (we use natural images from ImageNet [10]). Figure 4 shows reconstruction results on different images (and their corresponding ground-truths).

Table 2 shows the performance (in terms of CD) of different methods. Following previous work [42, 47], we show results in three categories.

In both metrics, our approach achieves state-of-the-art results. As before, our reconstruction network, contrary to other methods, does not make use of depths, surface normals, silhouette nor it exploits any form of multiview consistency. Instead, we make use of unlabeled natural images, which are very easy to obtain. Furthermore, we use a much simpler encoder-decoder architecture. We also note that OGN [40] uses a much more complex decoder (based on octrees) and considers much higher resolution volumetric occupancy ground-truths during training.

We note that the two novelties of our approach are complementary to previous works and thus could potentially be integrated with those methods for further performance gain.

### 4.3. Analyzing the Loss

Here, we perform an ablation study to see how our method performs with respect to the different loss terms. Table 3 shows the results of our method in both datasets when considering: (i) only the reconstruction loss ( $\mathcal{L}_{rec}$ ), (ii) the reconstruction and the shape prior losses ( $\mathcal{L}_{rec}$  and  $\mathcal{L}_{shape}$ ), (iii) the reconstruction and the image domain-confusion losses ( $\mathcal{L}_{rec}$  and  $\mathcal{L}_{img}$ ) and (iv) the full loss. In PASCAL 3D+, we show results in all seven categories considered.



Figure 4: 3D reconstruction from single image on PASCAL 3D+ [50]. For each image, we show the predicted and ground-truth (left) voxel representation (right). We show two different views for each 3D representation.

	chair	car	plane	average
3D-R2N2[8]	0.238	0.305	0.305	0.284
DRC [42]	0.158	0.099	0.112	0.122
OGN [40]	-	0.087	-	-
ShapeHD [47]	0.137	0.129	0.094	0.119
RAN	0.105	0.101	0.108	0.104

Table 2: Single-view 3D reconstruction results on Pasca3D+. We show results on CD metrics. DRC and ShapeHD use depth/normal/silhouettes as extra information during training. Our approach only considers (easily available) natural images. OGN considers a much stronger decoder and much higher voxel resolution. We show competitive results in both metrics.

We first observe that, for both datasets, each loss term has a positive impact on the the final reconstruction result. The shape prior loss alone is not sufficient to significantly improve the performance. However, the domain confusion loss alone already provides a substantial boost in performance. Finally, the model achieves its best performance when combining both constraints at the same time. These results therefore confirm that each of the proposed loss terms is critical in obtaining the final performance.

#### 4.4. Analyzing the Learned Representations

**Feature Visualization.** We use t-SNE [43] to visualize feature representations from different domains and at different adaptation stages. Figure 5(a-b) and Figure 6(a-b) show embeddings for Pix3D and PASCAL3D+, respectively. These figures contain t-SNE features from synthetic (blue) and real (red) images before and after adaptation, respectively. Figure 5(c-d) and Figure 6(c-d) show embeddings of 2D rendered images (blue) and points from the learned shape manifold, *i.e.*, latent representations from the shape autoencoder (yellow).

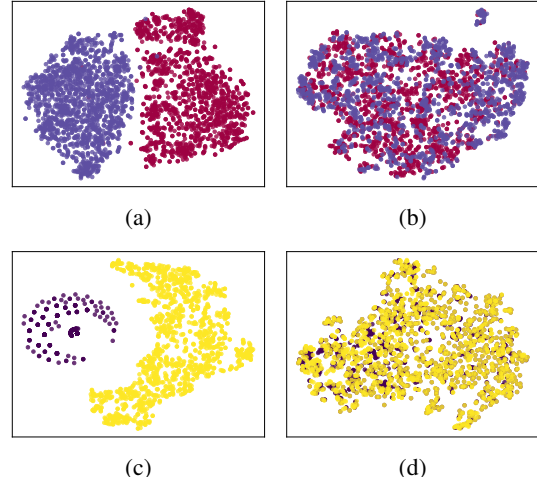


Figure 5: t-SNE visualization on Pix3D. (a-b) Rendered and natural image embeddings before and after domain confusion. (c-d) 2d rendered embedding and points from manifold before and after training.

In all cases, we can see that features become much more domain-invariant after training, as desired. During our experiments, we indeed observed a strong correspondence between reconstruction performance (on natural images) and the overlap between the different feature distributions.

**Shape interpolation.** In Figure 7, we show results of interpolating between two natural images of different shapes. We first transform each image into its latent representation. Then, we walk through the shape manifold and reconstruct the shape at different interpolated representations. We show qualitatively that the learned shape manifold gives smooth transition between the two object shapes.

**Shape arithmetic.** Another way to probe the learned representations is to show arithmetic on the latent space. Pre-

$\mathcal{L}_{rec}$	$\mathcal{L}_{img}$	$\mathcal{L}_{shape}$	Pix3D chair	plane	bus	car	Pascal 3D+					
				.202	.268	.280	.268	chair	mbike	train	tv	avg.
✓				.200	.294	.261	.239	.193	.248	.312	.221	.252
✓		✓		.151	.113	.096	.117	.141	.232	.105	.224	.147
✓	✓	✓		.136	.108	.088	.101	.105	.135	.111	.228	.125

Table 3: The performance of our model (on CD) considering different loss terms. We note the importance of each loss component on both metrics, although the shape prior loss alone does not give considerable improvement.

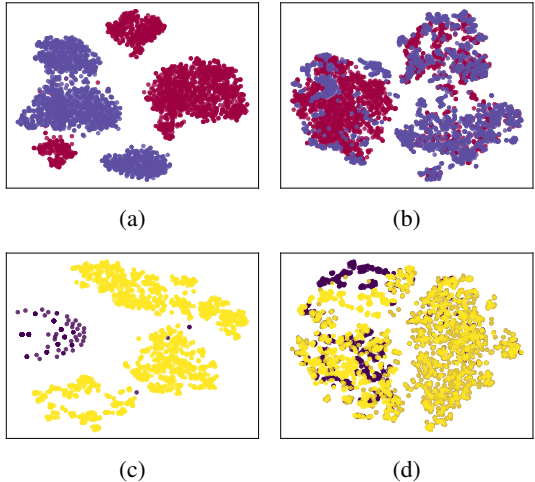


Figure 6: t-SNE visualization on PASCAL3D+. (a-b) Rendered and natural image embeddings before and after domain confusion. (c-d) 2d rendered embedding and points from manifold before and after training.

vious work [8, 46, 53] showed they are able to learn a semantic manifold of shapes in its latent space and arithmetic is done in samples from this space. In Figure 8, we perform shape arithmetic on different natural images. We first map them to the learned shape manifold (where arithmetical operations are done), then we reconstruct its shape. We observe that the representation after the arithmetic operations are still reasonable to reconstruct a realistic shape.

## 5. Conclusion

In this paper, we presented a framework for improved 3D reconstruction from single-view natural image. Our method leverages adversarial training and shape priors in two different ways. First it imposes learned features to be domain-invariant to help with the problem of domain adaptation. Second, we force the learned representations to lie in a rich shape prior manifold, imposing the reconstructions to be realistic. By using only RGB signal and with a much simpler network architecture, our model achieves competitive performance with the state of the art.

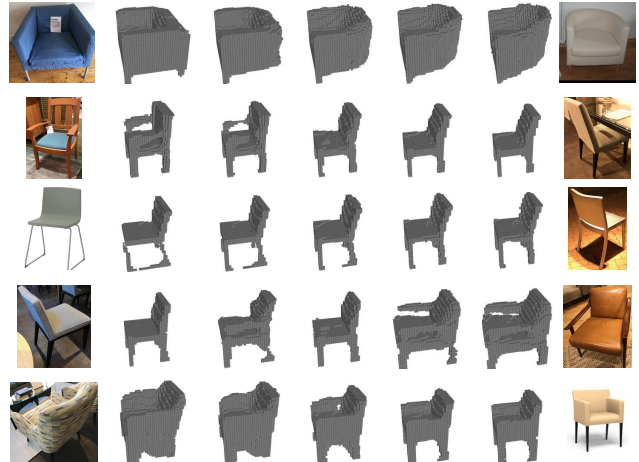


Figure 7: Shape interpolation from natural images.



Figure 8: Shape arithmetic from natural images. The top row show that ‘curviness’ vector can be added to other chairs. The other rows show that ‘arm’ vector can be added to other chairs.

## References

- [1] S. Ben-David, J. Blitzer, K. Crammer, A. Kulesza, F. Pereira, and J. W. Vaughan. A theory of learning from different domains. *Machine Learning*, 2010. 3
- [2] S. Ben-David, J. Blitzer, K. Crammer, and F. Pereira. Analysis of representations for domain adaptation. In *NIPS*, 2007.

- <sup>3</sup>
- [3] V. Blanz and T. Vetter. A morphable model for the synthesis of 3d faces. In *SIGGRAPH*, 1999. <sup>3</sup>
  - [4] J. S. D. Bonet and P. A. Viola. Roxels: Responsibility weighted 3d volume reconstruction. In *ICCV*, 1999. <sup>1, 2</sup>
  - [5] J. Bridle. Probabilistic interpretation of feedforward classification network outputs, with relationships to statistical pattern recognition. *Neurocomputing: Algorithms, Architectures and Applications*, 1990. <sup>5</sup>
  - [6] A. Broadhurst, T. Drummond, and R. Cipolla. A probabilistic framework for space carving. In *ICCV*, 2001. <sup>1, 2, 3</sup>
  - [7] A. X. Chang, T. A. Funkhouser, L. J. Guibas, P. Hanrahan, Q.-X. Huang, Z. Li, S. Savarese, M. Savva, S. Song, H. Su, J. Xiao, L. Yi, and F. Yu. Shapenet: An information-rich 3d model repository. In *CoRR*, 2015. <sup>1, 5</sup>
  - [8] C. B. Choy, D. Xu, J. Gwak, K. Chen, and S. Savarese. 3dr2n2: A unified approach for single and multi-view 3d object reconstruction. In *ECCV*, 2016. <sup>1, 2, 6, 7, 8</sup>
  - [9] G. Csurka. A comprehensive survey on domain adaptation for visual applications. In *Domain Adaptation in Computer Vision Applications*, Advances in Computer Vision and Pattern Recognition. Springer, 2017. <sup>2</sup>
  - [10] J. Deng, W. Dong, R. Socher, L.-J. Li, K. Li, and L. Fei-Fei. ImageNet: A Large-Scale Hierarchical Image Database. In *CVPR*, 2009. <sup>5, 6</sup>
  - [11] S. M. A. Eslami, D. J. Rezende, F. Besse, F. Viola, A. S. Morcos, M. Garnelo, A. Ruderman, A. A. Rusu, I. Danihelka, K. Gregor, D. P. Reichert, L. Buesing, T. Weber, O. Vinyals, D. Rosenbaum, N. C. Rabinowitz, H. King, C. Hillier, M. M. Botvinick, D. Wierstra, K. Kavukcuoglu, and D. Hassabis. Neural scene representation and rendering. *Science*, 2018. <sup>3</sup>
  - [12] M. Everingham, S. M. Eslami, L. Gool, C. K. Williams, J. Winn, and A. Zisserman. The pascal visual object classes challenge: A retrospective. *IJCV*, 2015. <sup>6</sup>
  - [13] H. Fan, H. Su, and L. J. Guibas. A point set generation network for 3d object reconstruction from a single image. In *CVPR*, 2017. <sup>2, 5, 6</sup>
  - [14] Y. Furukawa and C. Hernndez. Multi-view stereo: A tutorial. *Foundations and Trends in Computer Graphics and Vision*, 2015. <sup>1, 2</sup>
  - [15] Y. Ganin, E. Ustinova, H. Ajakan, P. Germain, H. Larochelle, F. Laviolette, M. Marchand, and V. S. Lempitsky. Domain-adversarial training of neural networks. *JMLR*, 2016. <sup>2, 3, 4</sup>
  - [16] R. Girdhar, D. F. Fouhey, M. Rodriguez, and A. Gupta. Learning a predictable and generative vector representation for objects. In *ECCV*, 2016. <sup>1, 2, 3</sup>
  - [17] I. Goodfellow, Y. Bengio, and A. Courville. *Deep Learning*. The MIT Press, 2016. <sup>1</sup>
  - [18] I. Goodfellow, J. Pouget-Abadie, M. Mirza, B. Xu, D. Warde-Farley, S. Ozair, A. Courville, and Y. Bengio. Generative adversarial nets. In *NIPS*, 2014. <sup>2, 3</sup>
  - [19] T. Groueix, M. Fisher, V. G. Kim, B. C. Russell, and M. Aubry. Atlasnet: A papier-mâché approach to learning 3d surface generation. *CVPR*, 2018. <sup>5, 6</sup>
  - [20] J. Gwak, C. B. Choy, A. Garg, M. Chandraker, and S. Savarese. Weakly supervised generative adversarial networks for 3d reconstruction. In *3DV*, 2017. <sup>2, 3</sup>
  - [21] K. He, X. Zhang, S. Ren, and J. Sun. Deep residual learning for image recognition. In *CVPR*, 2016. <sup>5</sup>
  - [22] D. Jimenez Rezende, S. M. A. Eslami, S. Mohamed, P. Battaglia, M. Jaderberg, and N. Heess. Unsupervised learning of 3d structure from images. In *NIPS*, 2016. <sup>1, 2, 3</sup>
  - [23] A. Kanazawa, S. Tulsiani, A. A. Efros, and J. Malik. Learning category-specific mesh reconstruction from image collections. In *ECCV*, 2018. <sup>2</sup>
  - [24] A. Kar, S. Tulsiani, J. Carreira, and J. Malik. Category-specific object reconstruction from a single image. In *CVPR*, 2015. <sup>1, 2, 3</sup>
  - [25] D. P. Kingma and J. Ba. Adam: A method for stochastic optimization. *ICLR*, 2014. <sup>4</sup>
  - [26] Z. Kourtzi and C. E. Connor. Neural representations for object perception: structure, category, and adaptive coding. *Annual review of neuroscience*, 2011. <sup>1</sup>
  - [27] A. Kundu, Y. Li, and J. M. Rehg. 3d-rcnn: Instance-level 3d object reconstruction via render-and-compare. In *CVPR*, 2018. <sup>2</sup>
  - [28] A. Laurentini. The visual hull concept for silhouette-based image understanding. *PAMI*, 1994. <sup>1, 2</sup>
  - [29] Y. Lecun, L. Bottou, Y. Bengio, and P. Haffner. Gradient-based learning applied to document recognition. In *Proceedings of the IEEE*, 1998. <sup>2</sup>
  - [30] Y. Li, H. Su, C. R. Qi, N. Fish, D. Cohen-Or, and L. J. Guibas. Joint embeddings of shapes and images via cnn image purification. *ACM Trans. Graph.*, 2015. <sup>3</sup>
  - [31] V. Nair and G. E. Hinton. Rectified linear units improve restricted boltzmann machines. In *ICML*, 2010. <sup>4</sup>
  - [32] D. Novotný, D. Larlus, and A. Vedaldi. Learning 3d object categories by looking around them. In *ICCV*, 2017. <sup>1</sup>
  - [33] P. O. Pinheiro. Unsupervised domain adaptation with similarity learning. In *CVPR*, 2018. <sup>2</sup>
  - [34] K. Saito, Y. Ushiku, T. Harada, and K. Saenko. Adversarial dropout regularization. In *ICLR*, 2018. <sup>2</sup>
  - [35] K. Saito, K. Watanabe, Y. Ushiku, and T. Harada. Maximum classifier discrepancy for unsupervised domain adaptation. In *CVPR*, 2018. <sup>2</sup>
  - [36] K. Saito, S. Yamamoto, Y. Ushiku, and T. Harada. Open set domain adaptation by backpropagation. In *ECCV*, 2018. <sup>2</sup>
  - [37] S. M. Seitz, B. Curless, J. Diebel, D. Scharstein, and R. Szeliski. A comparison and evaluation of multi-view stereo reconstruction algorithms. In *CVPR*, 2006. <sup>1, 2</sup>
  - [38] X. Sun, J. Wu, X. Zhang, Z. Zhang, C. Zhang, T. Xue, J. B. Tenenbaum, and W. T. Freeman. Pix3d: Dataset and methods for single-image 3d shape modeling. In *CVPR*, 2018. <sup>1, 5, 6</sup>
  - [39] M. Tatarchenko, A. Dosovitskiy, and T. Brox. Multi-view 3d models from single images with a convolutional network. In *ECCV*, 2016. <sup>1</sup>
  - [40] M. Tatarchenko, A. Dosovitskiy, and T. Brox. Octree generating networks: Efficient convolutional architectures for high-resolution 3d outputs. In *ICCV*, 2017. <sup>6, 7</sup>
  - [41] A. Torralba and A. A. Efros. Unbiased look at dataset bias. In *CVPR*, 2011. <sup>2, 3</sup>
  - [42] S. Tulsiani, T. Zhou, A. A. Efros, and J. Malik. Multi-view supervision for single-view reconstruction via differentiable ray consistency. In *CVPR*, 2017. <sup>1, 2, 6, 7</sup>

- [43] L. van der Maaten and G. Hinton. Visualizing data using t-SNE. *JMLR*, 2008. 7
- [44] S. Vicente, J. a. Carreira, L. Agapito, and J. Batista. Reconstructing pascal voc. In *CVPR*, 2014. 2
- [45] J. Wu, Y. Wang, T. Xue, X. Sun, B. Freeman, and J. Tenenbaum. Marrnet: 3d shape reconstruction via 2.5d sketches. In *NIPS*, 2017. 1, 2, 6
- [46] J. Wu, C. Zhang, T. Xue, B. Freeman, and J. Tenenbaum. Learning a probabilistic latent space of object shapes via 3d generative-adversarial modeling. In *NIPS*, 2016. 1, 2, 3, 6, 8
- [47] J. Wu, C. Zhang, X. Zhang, Z. Zhang, W. T. Freeman, and J. B. Tenenbaum. Learning shape priors for single-view 3d completion and reconstruction. In *ECCV*, 2018. 1, 2, 3, 4, 5, 6, 7
- [48] Z. Wu, S. Song, A. Khosla, F. Yu, L. Zhang, X. Tang, and J. Xiao. 3d shapenets: A deep representation for volumetric shapes. In *CVPR*, 2015. 2, 3
- [49] Y. Xiang, W. Kim, W. Chen, J. Ji, C. Choy, H. Su, R. Mottaghi, L. Guibas, and S. Savarese. Objectnet3d: A large scale database for 3d object recognition. In *ECCV*, 2016. 1
- [50] Y. Xiang, R. Mottaghi, and S. Savarese. Beyond pascal: A benchmark for 3d object detection in the wild. In *WACV*, 2014. 1, 5, 6, 7
- [51] Y. Yamane, E. T. Carlson, K. C. Bowman, Z. Wang, and C. E. Connor. A neural code for three-dimensional object shape in macaque inferotemporal cortex. *Nature Neuroscience*, 2008. 1
- [52] X. Yan, J. Yang, E. Yumer, Y. Guo, and H. Lee. Perspective transformer nets: Learning single-view 3d object reconstruction without 3d supervision. In *NIPS*, 2016. 1, 2
- [53] G. Yang, Y. Cui, S. Belongie, and B. Hariharan. Learning single-view 3d reconstruction with limited pose supervision. In *ECCV*, 2018. 1, 2, 8